Response to perturbations as a built-in feature in a mathematical model for paced finger tapping

Claudia R. González
Universidad Nacional de Quilmes, Departamento de Ciencia y Tecnología, Laboratorio de Dinámica Sensomotora, Bernal, Argentina

M. Luz Bavassi
Universidad de Buenos Aires, Instituto de Fisiología, Biología Molecular y Neurociencias (IFIByNE), Buenos Aires, Argentina and CONICET, Buenos Aires, Argentina

Rodrigo Laje*
Universidad Nacional de Quilmes, Departamento de Ciencia y Tecnología, Laboratorio de Dinámica Sensomotora, Bernal, Argentina and CONICET, Buenos Aires, Argentina

(Received 12 August 2019; published 20 December 2019)

Paced finger tapping is one of the simplest tasks to study sensorimotor synchronization. The subject is instructed to tap in synchrony with a periodic sequence of brief tones, and the time difference (called asynchrony) between each response and the corresponding stimulus is recorded. Despite its simplicity, this task helps to unveil interesting features of the underlying neural system and the error-correction mechanism responsible for synchronization. Perturbation experiments are usually performed to probe the subject's response, for example, in the form of a "step change," i.e., an unexpected change in tempo. The asynchrony is the usual observable in such experiments and it is chosen as the main variable in many mathematical models that attempt to describe the phenomenon. In this work we show that although asynchrony can be perfectly described in operational terms, it is not well defined as a model variable when tempo perturbations are considered. We introduce an alternative variable and a mathematical model that intrinsically takes into account the perturbation and make theoretical predictions about the response to novel perturbations based on the geometrical organization of the trajectories in phase space. Our proposal is relevant to understand interpersonal synchronization and the synchronization to nonperiodic stimuli.

DOI: 10.1103/PhysRevE.100.062412

I. INTRODUCTION

Sensorimotor synchronization (SMS), that is, the ability to synchronize our movement to a periodic external stimulus, underlies specifically human behaviors like music and dance [1] and involves time processing in the *millisecond timing* range (i.e., hundreds of milliseconds [2]). SMS is a rare ability among animals and it apparently correlates with the also rare ability of vocal learning [3–5], with potential evolutionary implications (although see Sec. 2.5.2 in Ref. [6]). The simplest task to study this behavior is paced finger tapping, where a subject is instructed to tap in synchrony with a periodic sequence of brief stimuli (for instance, tones or flashes) like keeping pace with music and while registering the occurrence time of every response. The natural observable and one of the variables most used to quantify the behavior [6,7] is the difference between the occurrence times of every response (R_n) and the corresponding stimulus (S_n), called synchrony error or simply asynchrony:

$$e_n = R_n - S_n. \tag{1}$$

The asynchrony of a single trial is a relatively noisy time series with a standard deviation of up to a few tens of milliseconds (Fig. 1). Despite that none of the e_n are zero, most people can achieve average synchronization with a mean value that is typically negative (called negative mean ssynchrony or NMA, hypothetically representing the point of subjective synchrony) [8]. The main goal is to understand how the brain can maintain average synchrony or recover it after a perturbation.

The number of theoretical and experimental works dedicated to understand this behavior and its neural bases is rapidly growing, especially imaging and electrophysiology studies like electroencephalography (EEG), magnetoencephalography (MEG), and functional Magnetic Resonance Imaging (fMRI) [9–16]. It is very simple to show that there is an error-correction mechanism in the brain in charge of keeping average synchrony that operates based on past performance [1,17]. On the theoretical side [17,18], such a mechanism is easily conceptualized as a map or difference equation for the observable e_n:

$$e_{n+1} = f(e_n, T_n) + \text{noise}, \tag{2}$$

where the asynchrony at the next step e_{n+1} depends on its previous value e_n (or several previous values in some models [19]) and probably on some parameter like the sequence period or interstimulus interval T_n:

$$T_n = S_n - S_{n-1}. \tag{3}$$

*Corresponding author: rlaje@unq.edu.ar

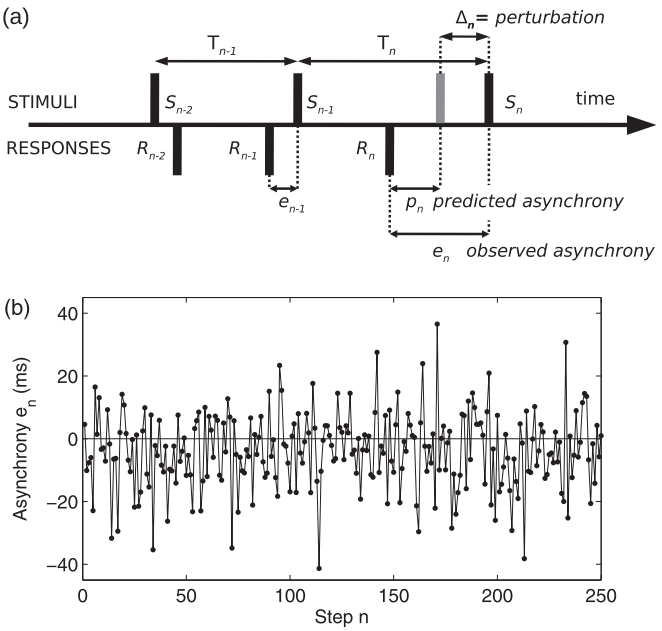

FIG. 1. (a) Schematic description of the task, variables, and parameters. A perturbation occurs at step n. (b) Isochronous sequence from one subject (single trial, no averaging). Mean = 3.9 ms, SD = 12.1 ms.

Studies that aim at finding a linear correction function f make use of mean values, standard deviations, and autocorrelation functions and thus they analyze synchronization to periodic stimuli sequences without any perturbation [19]; periodic sequences are also used by works that study the structure of the noise term [20]. Alternatively, in order to find the best correction function f that is the deterministic part of the equation one can perform perturbations to an otherwise isochronous sequence and analyze the resynchronization [17]. That is the approach we chose.

The main variable for quantifying the behavior, the asynchrony e_n, is always operationally well defined according to Eq. (1) and Fig. 1. In this work, however, we show that e_n is an ill-defined variable in terms of a map or difference equation when the stimulus sequence has perturbations. This issue is relevant not only during a controlled perturbation experiment in a laboratory setting but also in a more natural, ecological setting like music performance where the stimulus sequence is not strictly periodic (e.g., a choir or orchestra conductor performing a ralentando) or when the stimulus sequence is intrinsically variable (e.g., interpersonal synchronization where the stimulus sequence is the other person's production). We propose an alternative variable and a mathematical model that reproduces the observed data including the effect of perturbation and make theoretical predictions.

II. RESULTS

A. Predicted versus observed asynchrony

From a behavioral point of view, one of the approaches to unveil the form of the error-correction mechanism in a paced finger-tapping task is to find the best correction function $f(e_n)$ [Eq. (2)] that, based on the observed asynchrony e_n [Eq. (1)] and the interstimulus interval T_n [Eq. (3)], predicts the asynchrony at the next step. Figure 1 shows a graphical definition of all variables and parameters.

According to Eq. (1), the asynchrony e_n takes as a reference point the occurrence time of the stimulus S_n. The traditional way of perturbing the system is to unexpectedly modify the stimulus period, which is done by shifting in time one or several consecutive stimuli, i.e., modifying S_n (and perhaps the following stimuli too; see Fig. 1). An example is the "step-change" perturbation, where the stimulus period changes unexpectedly by a fixed amount Δ from a given stimulus S_n on (in musical terms it is a sudden change in tempo). A critical issue that has been overlooked in the literature, both experimental and theoretical, is that the change of the occurrence time of the perturbed stimulus S_n is arbitrary and thus is not a well-defined time reference [21]. The consequence of this is that the variable e_n becomes ill defined because its value changes at the moment of perturbation but not because of its own dynamics. In other words, if an unexpected perturbation occurs at step n, then the actual asynchrony will be different from the value predicted by the subject (or the model) because the corresponding stimulus was shifted by an arbitrary amount equal to the size of the perturbation.

In this work we propose the following way to resolve this issue: We distinguish between the *predicted* asynchrony value p_n and the actually *observed* asynchrony value e_n (Fig. 1). If a change in period occurs at step n:

$$\Delta_n = T_n - T_{n-1}, \tag{4}$$

then the predicted asynchrony p_n and the actually observed asynchrony e_n are related by the following expression:

$$p_n = e_n + \Delta_n. \tag{5}$$

It is important to note that Eq. (5) is not a theoretical assumption but the actual relationship between the variables. Note also that if no perturbation occurs, then $\Delta_n = 0$ and thus $p_n = e_n$.

Taking this distinction into account, a model like Eq. (2) must be written as (discarding the noise term for simplicity):

$$p_{n+1} = f(e_n, T_n) \tag{6}$$

and by using Eq. (5) we can get a closed model for the variable p_n:

$$p_{n+1} = f(p_n - \Delta_n, T_n). \tag{7}$$

We can always go back to the observed asynchrony e_n by means of Eq. (5).

B. Model implementation

In this section we proposed an improved model based on our previous work and apply the distinction proposed above.

1. Previous work

In Ref. [17] we showed that nonlinear effects are important even for small perturbations of 10% of the period. There are two main effects when step change perturbations are performed. First, if the tempo is made faster [negative perturbation $\Delta_n < 0$; Fig. 2(a)], then the resynchronization is monotonic until a new baseline is reached; however, if

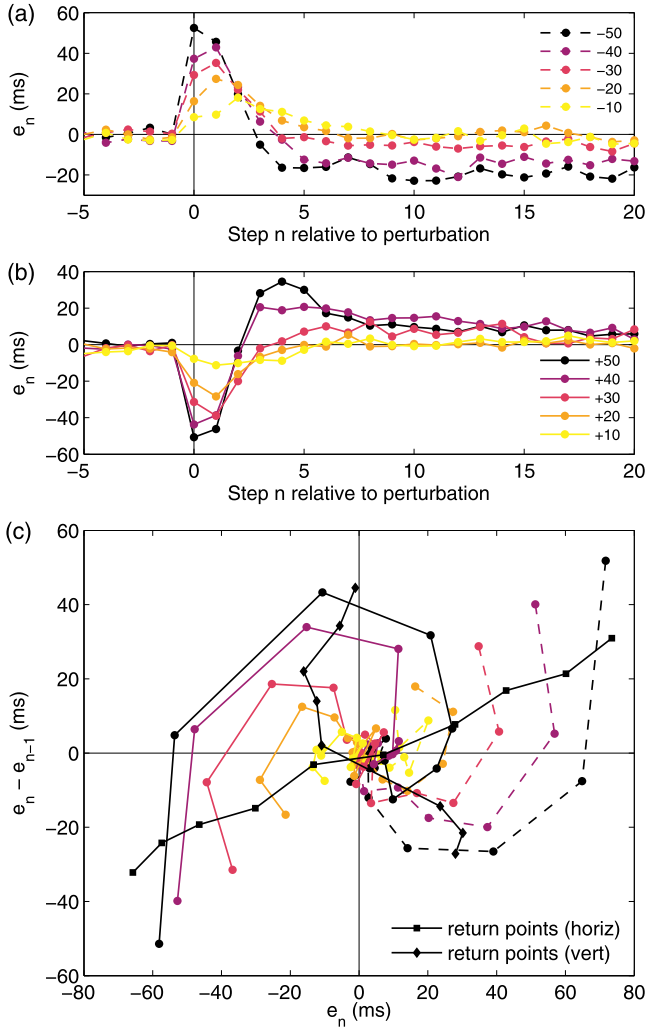

FIG. 2. Experimental time series and phase-space reconstruction (all experimental data shown in this work were published in Ref. [17]). Perturbation sizes are in milliseconds and the preperturbation period is $T_0 = 500$ ms. (a) Negative step changes. (b) Positive step changes. (c) Phase-space reconstruction by embedding the time series above. Note that there is a common region of phase space shared by trajectories from large opposite perturbations (most notably +50 and −20 trajectories). Black curves are the estimated return points.

the tempo is made slower [positive perturbation $\Delta_n > 0$; Fig. 2(b)], then the asynchrony overshoots before reaching the new baseline. The existence of the overshoot makes it necessary to introduce a second variable x_n—otherwise, the deterministic nature of the model would be violated [17,22]. Second, the asymmetry of the response in front of symmetric perturbations requires the introduction of nonlinear terms of even order (e.g., quadratic). In order to correctly reproduce these two observations we have proposed a two-variable, nonlinear model:

$$\begin{aligned} e_{n+1} &= a\, e_n + b(x_n - T_n) + F(e_n, x_n, T_n) \\ x_{n+1} &= c\, e_n + d(x_n - T_n) + T_n + G(e_n, x_n, T_n), \end{aligned} \tag{8}$$

where F and G are nonlinear functions of their arguments. An extensive discussion about modeling choices and nonlinear behavior in finger-tapping tasks can be found in our previous work [17].

2. *New evidence and improved model*

Before introducing the distinction between predicted and observed asynchrony, we propose improved functions F and G based on new experimental evidence. We take the experimental data of step change perturbations from Ref. [17] and reanalyze them as follows. First we perform an embedding of the time series shown in Figs. 2(a) and 2(b) to reconstruct the qualitative geometrical arrangement of the underlying phase space [23]. Figure 2(c) shows the result, where we added the detection of return points for every trajectory (see methods in Appendix A 1).

The shape of the curve of return points of a map gives us information about the underlying system, meaning whether linear or quadratic or cubic terms, etc., are needed to model it (in much the same way as the nullclines of a flow do; see discussion in Appendix A 1). The geometrical organization of the return points in Fig. 2(c) shows a certain degree of asymmetry and saturation (especially for the vertical axis), which tells us that quadratic and cubic terms are needed. In a two-variable model there are six possible quadratic terms (e^2, x^2, ex for each equation) and eight possible cubic terms (e^3, e^2x, ex^2, x^3 for each equation), yet we want to use the smallest number of terms that correctly represent the behavior. However, we cannot use normal form theory to choose among the nonlinear terms because within the regime analyzed in this work (synchronization to a periodic sequence or resynchronization following a tempo step change of fixed size) the behavior does not show any bifurcations but a robust convergence to a single fixed point representing average synchrony [17,24–26]. After testing many combinations of nonlinear terms with qualitatively similar results, we choose the following:

$$\begin{aligned} F(e_n, x_n, T_n) &= \alpha e_n^3 + \beta e_n (x_n - T_n)^2 + \gamma (x_n - T_n)^3 \\ G(e_n, x_n, T_n) &= \delta e_n^2. \end{aligned} \tag{9}$$

In Sec. II C we display a summary of the obtained phase spaces with our selection of nonlinear terms. We emphasize that our choice of nonlinear terms is not unique—it is not possible to solve for unique F and G from the shape of the return points in the embedding.

Now we incorporate the distinction between predicted and observed asynchrony. According to the previous subsection we must substitute $e_{n+1} \to p_{n+1}$ and $e_n \to p_n - \Delta_n$:

$$\begin{aligned} p_{n+1} &= a\,(p_n - \Delta_n) + b(x_n - T_n) + F(p_n - \Delta_n, x_n, T_n) \\ x_{n+1} &= c\,(p_n - \Delta_n) + d(x_n - T_n) + T_n + G(p_n - \Delta_n, x_n, T_n) \end{aligned} \tag{10}$$

and to get a closed system we define the auxiliary variable $s_{n+1} = T_n$. This leads us to

$$\begin{aligned} p_{n+1} &= a\,(p_n - (T_n - s_n)) + b(x_n - T_n) \\ &\quad + F(p_n - (T_n - s_n), x_n, T_n) \\ x_{n+1} &= c\,(p_n - (T_n - s_n)) + d(x_n - T_n) + T_n \\ &\quad + G(p_n - (T_n - s_n), x_n, T_n) \\ s_{n+1} &= T_n \end{aligned} \tag{11}$$

where F and G are defined according to Eq. (9). It is worth noting that T_n is a parameter whose value is up to the experimenter.

3. Parameter interpretation

It is always difficult to establish analogies or correlates between a behavioral model and the underlying processes in the brain. The reports of neural correlates and mechanisms in SMS are still very scarce, despite a growing literature (for a review see Ref. [6]). However, the way we model allows us to advance possible interpretations and make theoretical predictions leading to further experiments. The qualitative features of our model, Eqs. (11) and (9), can be interpreted as follows. Variable p can be interpreted as the representation in the brain of the predicted asynchrony, i.e., the predicted result of the error correction, while variable x can be interpreted as the representation of the interstimulus interval T. The linear coupling between them (parameters a, b, c, and d) can be interpreted as the way they influence each other at first order; e.g., $a > 0$ means that if the p percept is positive (tap lagging beep), then p shall decrease in the next step (tap closer to the beep), while $b > 0$ means that if the x percept is less than the current interstimulus interval, then p shall decrease in the next step, both as expected. Nonlinear terms are interesting in that they suggest mechanisms and restrictions. While the linear term ap means that asynchrony is corrected as a fraction of the previous asynchrony, the term αp^3 would mean that the rate of correction itself changes as a function of the asynchrony: $ap + \alpha p^3 = (a + \alpha p^2)p$. On the other hand, the cross-term $\beta p x^2$ might point to an interference between the two percepts, possibly due to shared resources or common circuits supporting p and x, bottleneck effects, etc. See Ref. [17] for further discussion and the next sections for predictions.

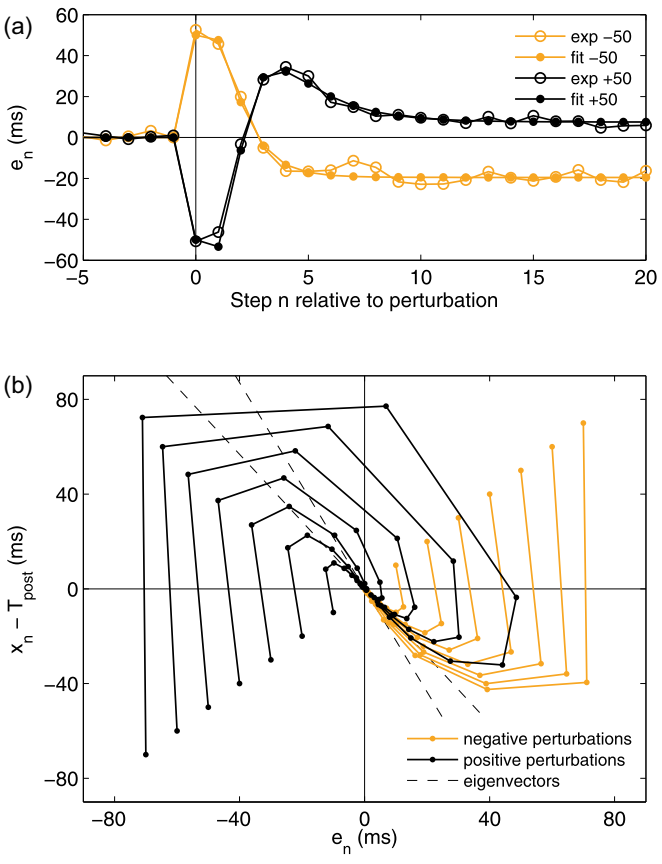

FIG. 3. Model fitting. (a) Experimental ±50-ms time series and model fitting results. (b) Model phase space. Response to perturbations occuring at $n = 0$, $\Delta_0 = \pm 10, \pm 20, \pm 30, \pm 40, \pm 50, \pm 60$, and ± 70 ms. Larger perturbations begin farther away from the origin (preperturbation steps not shown for visual clarity). Note the region of phase space that is shared between trajectories corresponding to positive and negative perturbations (upper right and lower right quadrants).

TABLE I. Fitted parameter values. All simulations in this work use this unique set of parameter values unless stated otherwise. Linear coefficients a, b, c, and d are nondimensional; quadratic coefficient δ has units of ms^{-1}; cubic coefficients α, β, and γ have units of ms^{-2}. The preperturbation interstimulus interval is $T_0 = 500$ ms.

$a = 0.981$	$\alpha = -2.21 \times 10^{-5}$
$b = 0.266$	$\beta = -7.84 \times 10^{-5}$
$c = -0.823$	$\gamma = 5.34 \times 10^{-5}$
$d = 0.0238$	$\delta = 3.35 \times 10^{-3}$

C. Model fitting, model simulations, and fitting analysis

As we did before [17], we use a genetic algorithm to fit the model [Eqs. (11) and (9)] to the experimental time series shown in Figs. 2(a) and 2(b); see methods in Appendix A 2. The results are shown in Fig. 3. The obtained parameter values are shown in Table I. The full fitting results (all perturbation sizes) are shown in Appendix A 3.

The fitting goodness is noteworthy, especially when compared to previous attempts in the literature with a similar or even greater number of parameters (for instance, our own previous work [17] and many others' work, e.g., Refs. [24–29]). It must be taken into account that, contrary to ours, modeling and fitting efforts in the finger-tapping literature usually perform separate fits for different perturbation sizes and types, effectively multiplying the number of parameters by a factor of 2 at least (effective 10-parameter model in Ref. [25]; effective 12-parameter model in Ref. [24]; effective 24-parameter mode in Ref. [27]; effective 72-parameter model in Ref. [28]). In addition, none of them included the perturbation in the modeling or the fitting.

In order to analyze the robustness of the fitting results we proceeded as follows. Every run of a genetic algorithm provides a solution that best fits the data according to the fitness function. As we describe in Appendix A 2 (also in our previous work [17]) we decided to run the algorithm 200 times to choose the absolute best among those 200 converged solutions. This, in addition, allows us to perform a statistical and dynamical analysis of all solutions. The distributions of obtained values for every parameter can be seen in Appendix A 4. Most of the distributions are unimodal, which speaks in favor of the robustness of the fitting procedure (Fig. 10). On the other hand, there is some interdependency between some of the linear parameters, i.e. a correlation

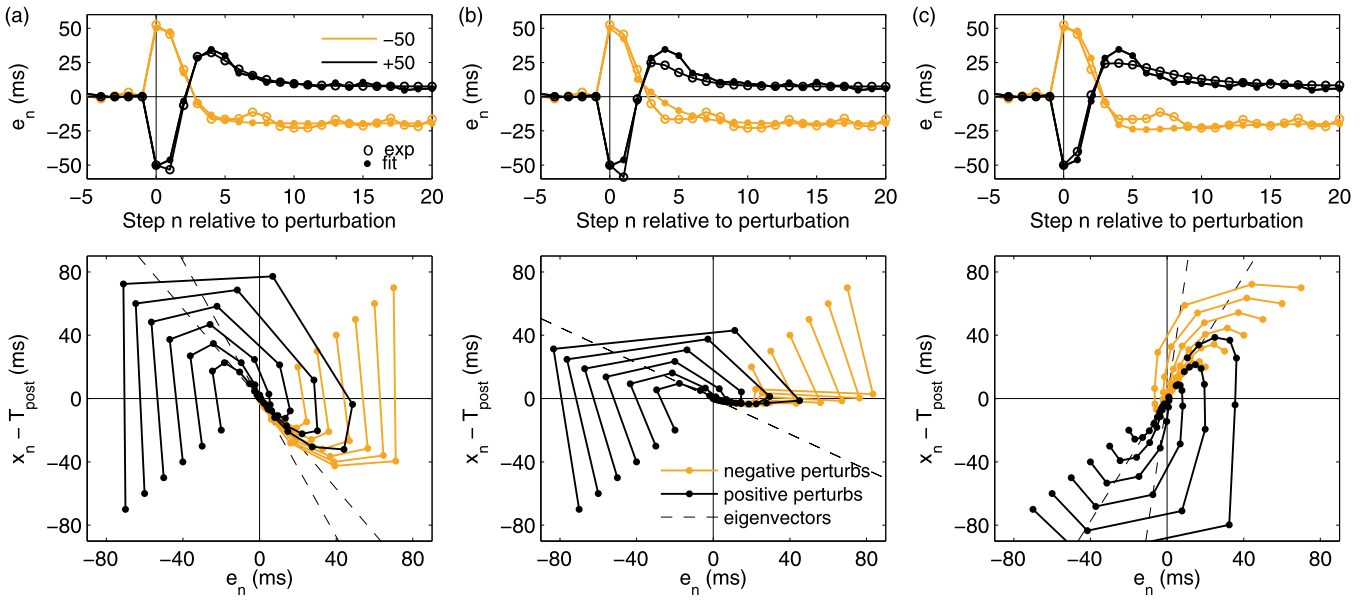

FIG. 4. Variety of solutions from the fitting procedure. (a) Type-I phase space and time series (58% of all solutions; the fittest solution of all, shown in Table I and Figs. 3, 5, 6, and 7, is this type). (b) Type-II phase space and time series (40% of all solutions; parameter values in Appendix A 5). (c) Type-III phase space and time series (2% of all solutions; parameter values in Appendix A 5).

between their converged values, for instance between b and c (Fig. 11). Nonlinear parameters are mostly uncorrelated (Fig. 12). Linear and nonlinear parameters are mostly uncorrelated, except perhaps among b, c, and α (Fig. 13). All this means that the model might be overparameterized and might fit the experimental time series with a smaller number of linear terms, but our choice of nonlinear terms is appropriate.

We plotted the phase space of every obtained solution and made an exhaustive visual search in order to qualitatively classify them. We found three types of phase portraits (Fig. 4). All have one hyperbolic equilibrium. Type I and III have two different eigenvalues and eigenvectors, and the flow rotates clockwise and counterclockwise, respectively; type II is a degenerate node (two equal eigenvalues and a single eigenvector) and the x variable has a particularly fast dynamics. The fittest of all 200 solutions is the set of parameter values shown in Table I and belongs to type I (that is the most frequent type of phase portrait, and the most frequent among the best solutions; the parameter values corresponding to types II and III are in Appendix A 5).

D. Benefits of the proposed approach

The most important feature of our model is that it incorporates the perturbations to the stimulus period in the modeling approach, leading to autonomous dynamics once the stimulus period sequence T_n is chosen as input. We achieved this by developing a closed equation for variable p_n [Eqs. (11) and (9)] based on a model-free relationship between p_n and the observable e_n [Eq. (5)]. An advantage of having a closed model with built-in perturbations is the ability to perform a bifurcation analysis on it, which is the subject of future work.

In the absence of bifurcations, as is the case in this work, our approach still offers advantages in the form of autonomous dynamics without any need to modify the value of the variable "by hand" whenever the stimulus period changes. This is illustrated in Fig. 5, where we show three common experimental manipulations of the stimulus period T_n [Fig. 5(a), step change; Fig. 5(b) sinusoidal variation; Fig. 5(c) random variation]. Once the stimulus period sequence is set (top row), our model evolves in time without any intervention from the experimenter (second row). The traditional way of doing this (third row) consists in considering the model without distinguishing between p_n and e_n, that is, Eq. (8), but this of course needs adjusting the value of the variable $e_n \to e_n - \Delta T$ by hand (shown in the figure as orange circles) every time there is a change in the parameter $T_n \to T_n + \Delta T$ to produce the correct time evolution (in the sinusoidal and random variations the experimenter needs to adjust e_n at every step). Finally, a naive version is shown in the bottom row where Eq. (8) is used without adjusting the value of e_n by hand.

Note that we decided to plot e_n instead of p_n throughout this work mainly for historical reasons so it is easier to compare to previous models' results and experimental results. Keep in mind, however, that all numerical simulations of our proposed model in this work were performed by solving the closed equation for p_n [Eq. (11) with nonlinear terms as in Eq. (9) and coefficient values as in Table I), and then translated $p_n \to e_n$ by means of Eq. (5).

E. Theoretical predictions

1. Geometrical organization of phase space

The geometrical arrangement of the trajectories in the experimental phase space [Fig. 2(c)] is remarkable in that the trajectories corresponding to the largest positive perturbations share a region of phase space during the overshoot with some of the trajectories of the negative perturbations (that do not have overshoot). This suggests that the error-correction mechanism in the brain might not distinguish between both

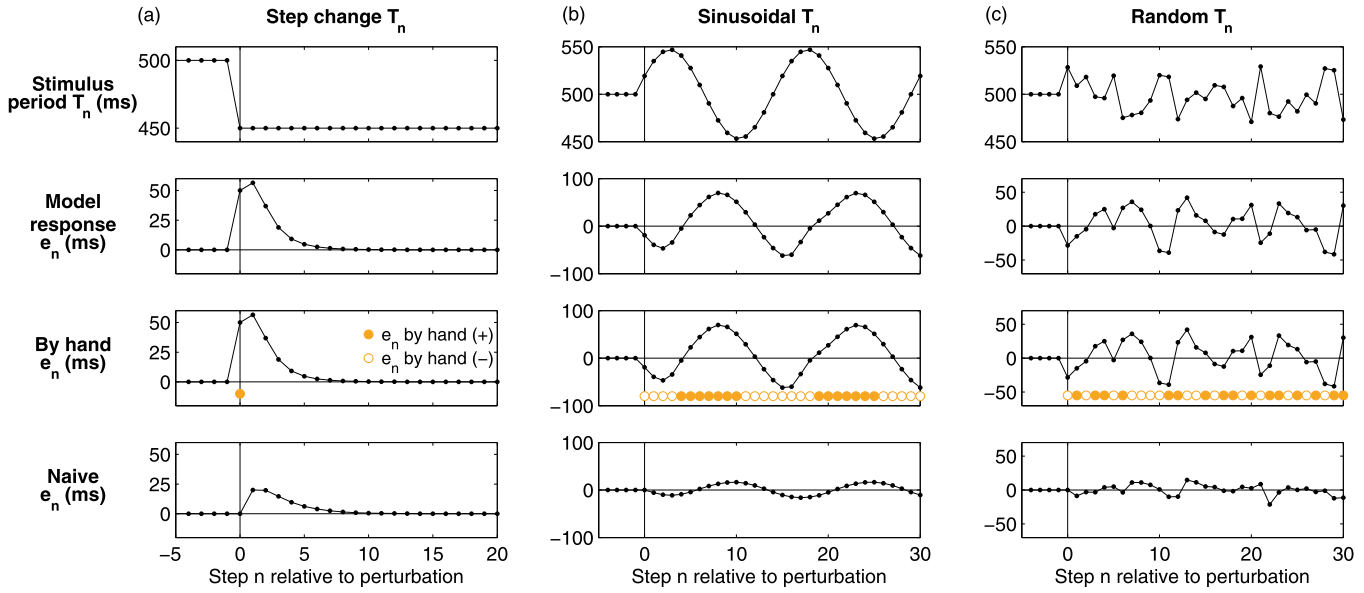

FIG. 5. Three common experimental manipulations of the stimulus period (top row) and response of our model (second row). (a) Step change in stimulus period. (b) Sinusoidal change. (c) Pseudorandom change. For comparison, the third row shows the behavior of the model when no distinction between predicted p_n and observed e_n is made, which is the traditional way of modeling where by-hand modification of e_n is needed (shown as orange filled circles when e_n must be increased and open circles when it must be decreased); fourth row shows a "naive" approach where neither distinction p_n/e_n nor by-hand modification are made.

types of trajectories while they are roughly in the same region of phase space. The approximate location of such region is clear and is labeled "B" in the bottom panel of Fig. 6(a) but corresponds to very different time instants in the time series (top panel).

The remarkable similarity between the experimental phase space [Fig. 2(c)] and the model phase space [Fig. 3(b)] should not be construed quantitatively as a measure of goodness but qualitatively as equivalent geometrical arrangements of the trajectories—both have trajectories with asymmetric

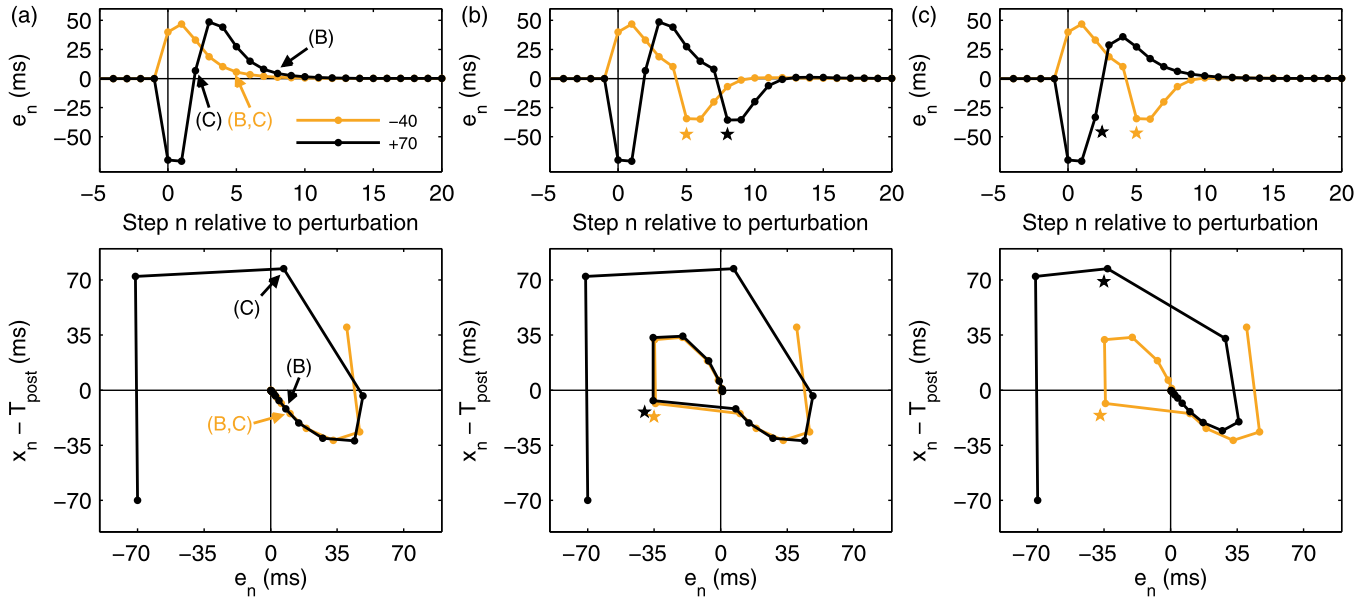

FIG. 6. Model predictions (I). (a) Response to a step change perturbation and choice of points for the second perturbation. Points labeled "B" and "C" have similar asynchrony values and correspond to the perturbations in panels (b) and (c), respectively. (b) Response to the proposed manipulation: Both conditions of perturbation 1 (−40- and +70-ms step changes) give similar responses to perturbation 2 (−40-ms variable only). The perturbed points are labeled with stars and correspond to the "B" label in panel (a). (c) Response to consecutive perturbations as in (b) but the second perturbation takes place in different points of phase space: The response after perturbation 2 depends on the condition of perturbation 1, despite having similar initial asynchrony values (positive control). The perturbed points are labeled with stars and correspond to the "C" label in panel (a).

overshoot and both have trajectories that share a common region in phase space despite coming from opposite perturbations. Our model allows us then to make the following prediction: A perturbation to the variable in the region labeled "B" in phase space [see Fig. 6(a)] should show the same postperturbation time evolution no matter what original trajectory it belongs to.

This prediction, however, must be tested carefully. For the very same reasons exposed in Sec. II A, in the history of paced finger-tapping experiments it has been intrinsically difficult to perturb the value of the stimulus period T_n without perturbing the variable e_n and, conversely, to perturb the variable without perturbing the stimulus period. In a recent work [21], however, we pointed at this overlooked issue and showed the feasibility of novel experimental manipulations to the variable only to avoid the confounding. Here we propose to use these novel perturbations to study the response of the model in front of two consecutive perturbations:

(i) first a traditional step change perturbation (in two conditions, positive and negative);

(ii) second, and while the resynchronization from the first perturbation takes place, a perturbation to the variable only (i.e., without changing the stimulus period).

Our prediction is that the time evolution following the second perturbation will be the same for both conditions (positive or negative first perturbation), provided the second perturbation is performed when the system is approximately in the same region of phase space. The rationale behind this proposal is that if we, on the contrary, performed two consecutive traditional step change perturbations, then we would not be able to resolve the following confounder: In case an overshoot appears in both conditions after the second perturbation it may be due either because our hypothesis is valid or because it is the known response to the (second) step change perturbation.

Numerical simulations supporting our prediction are in Fig. 6, where we show the results of [Fig. 6(a)] a single step change (negative control) and the definition of perturbation points; [Fig. 6(b)] the proposed manipulation; and [Fig. 6(c)] two consecutive perturbations as in Fig. 6(b) but performed in different points of phase space (positive control). In the consecutive perturbations [comparison of Figs. 6(b) and 6(c)] the time evolution after the second perturbation is either very similar between conditions [Fig. 6(b)] or different [Fig. 6(c)].

2. *Perturbations to the variable only*

Our second prediction is that the response to large-enough symmetric perturbations to the variable might be asymmetric. This can be seen in the phase space of Fig. 7, after noting that large negative perturbations (i.e., jump to the left) display an overshoot while large positive perturbations (i.e., jump to the right) do not. This would prove that a step change perturbation is not needed to display nonlinear behavior—perturbations to the variable without changing the stimulus period might elicit it, too, provided they are large enough. On the other hand, if the perturbation size is small enough, then the response to symmetric perturbations might look symmetric (see Fig. 7).

Last, the predictions described in this subsection and the previous subsection are valid if the perturbations are performed on time series displaying asymmetric overshoot; otherwise, conclusions would be flawed.

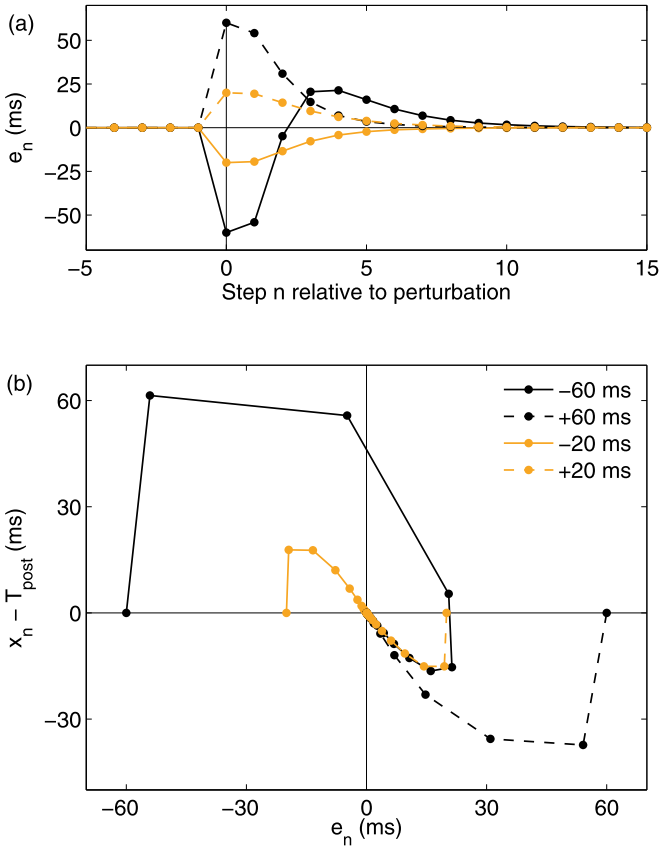

FIG. 7. Model predictions (II). Response to perturbations to the variable only (large: ±60 ms; small: ±20 ms). The response to large perturbations is asymmetric (i.e., it overshoots after the negative perturbation only); the response to small perturbations is mostly symmetric. (a) Asynchrony time series. (b) Trajectories in phase space.

3. *Generalization to other experimental paradigms*

Within our modeling approach, a step-change perturbation is the elemental perturbation: the stimulus period (the main parameter) is changed only once by a fixed amount. All other period perturbations can be understood as consecutive step-change perturbations [17]. This allows us to generalize the applicability of our model to other SMS phenomena like interpersonal synchronization. Here the stimuli sequence is the other person's production; it is of course naturally variable and can be considered a sequence of small, consecutive step-change perturbations. Our model takes any period perturbation into account as a built-in feature and could be a new tool to understand and conceptualize many findings in the field. This would be relevant also in group synchronization and leader-follower relationships (like in choirs and orchestras), as any naturally occurring variability in the timed actions of any participant or tempo change by the leader will act as a perturbation to the rest.

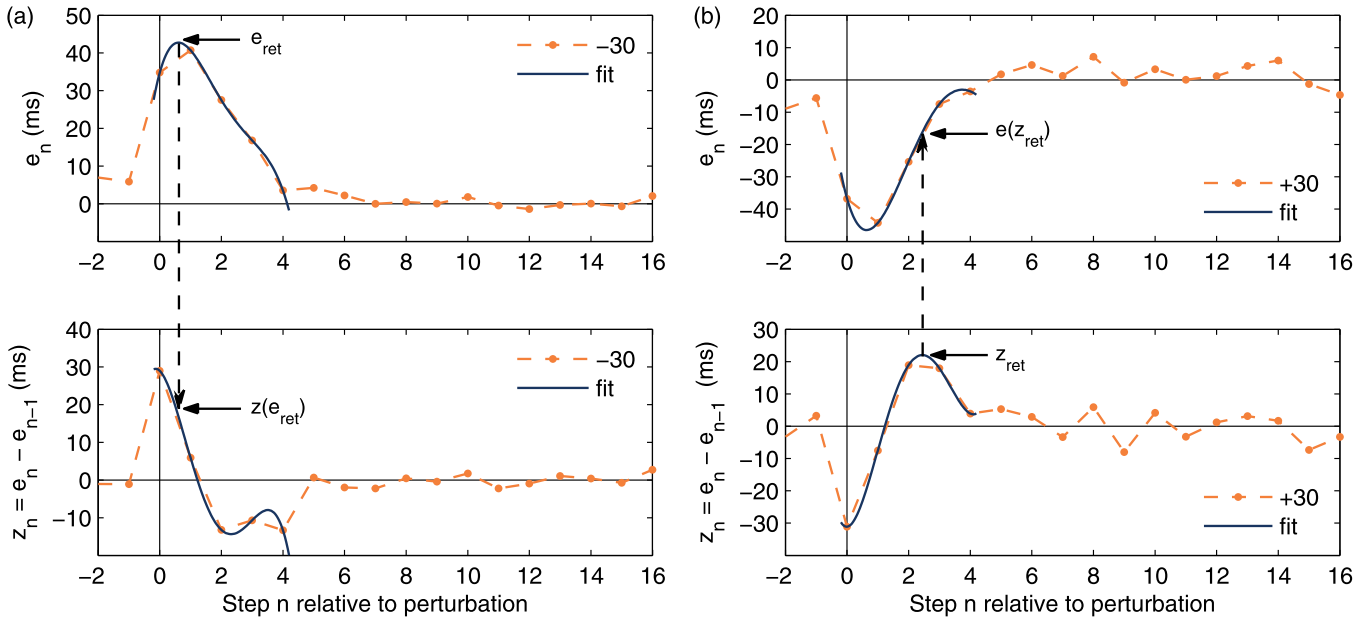

FIG. 8. Estimation of return points. (a) Return points of e_n (top panel; labeled "horiz" in Fig. 2(c)) and corresponding z_n value (bottom panel). (b) Return points of z_n [bottom panel; labeled "vert" in Fig. 2(c)] and corresponding e_n value (top panel).

III. CONCLUSIONS

We showed that the asynchrony e_n, the most important variable in the literature of paced finger-tapping experiments and theoretical models [6,7], is actually an ill-defined variable for a map or difference equation model when perturbations to the stimulus sequence are present. We proposed a distinction between predicted and actually observed asynchrony and developed the first mathematical model to solve the inherent ill definition. This is also the first mathematical model in sensorimotor synchronization that takes into account the response to a temporal perturbation as a built-in feature. Our own previous attempt [17], though successful at unifying, fell short of completely including the perturbation in the model dynamics.

Our model is able to fit the step change perturbation data remarkably well [Figs. 3(a) and 9], reproducing the response time series very accurately at all steps (including the perturbation step) with no modification of the variable "by hand" and with basically the same number of parameters than comparable models. It is only surprising that no published works so far in the paced finger-tapping literature, up to our knowledge, deal with the issue of ill definition of the main model variable when the sequence period is perturbed. On the other hand, models based on forced or coupled nonlinear oscillators [28,30–32], traditionally classified as belonging to a "dynamical systems" approach, are naturally well defined even in the presence of perturbations to the period.

Temporally displaced auditory feedback (either delayed or advanced) is also a usual way of probing the system [33–36] and it does not suffer from the issue of ill definition of the variable we addressed in this work. It remains to be shown, however, how it relates to changing the asynchrony in the models as it produces a modification in the asynchrony value but it also introduces a dissociation between auditory feedback and proprioceptive and tactile feedback [35].

We also showed that nonlinear behavior (asymmetry of responses) might be observed when the variable only is perturbed, i.e. even in the absence of a perturbation to the stimulus sequence, if the perturbation is large enough. Experimental perturbations like the ones proposed in Ref. [21] but with larger magnitudes are needed. We acknowledge that similar results can be obtained by using a different set of nonlinear terms, and this calls for more experimental data showing any kind of bifurcation in the behavior so as to choose the correct set of parameters via normal form theory.

Our model assumes, as many others, that the origin of the asynchrony is not important for keeping average synchrony or for achieving resynchronization. Qualitative features of resynchronization after a perturbation are thus similar independently of whether the asynchrony was produced by a perturbation to the parameter or to the variable or both. This is a common theoretical assumption in the literature only recently supported by experimental results [21].

Our theoretical results show that past (observed) and future (predicted) asynchronies play different roles in the model, and the remarkable fitting to the experimental data thus offers indirect evidence for a separate cerebral account of predicted versus actually observed asynchrony. Further experimental work is needed to decide whether this holds true.

ACKNOWLEDGMENTS

This work was supported by Universidad Nacional de Quilmes (Argentina), CONICET (Argentina), and The Pew Charitable Trusts (USA, Grant No. 2009-000360-006). C.R.G. and R.L. analyzed data, wrote code, and performed numerical simulations; R.L. conceptualized the work and developed the model; and C.R.G., M.L.B., and R.L. wrote the manuscript.

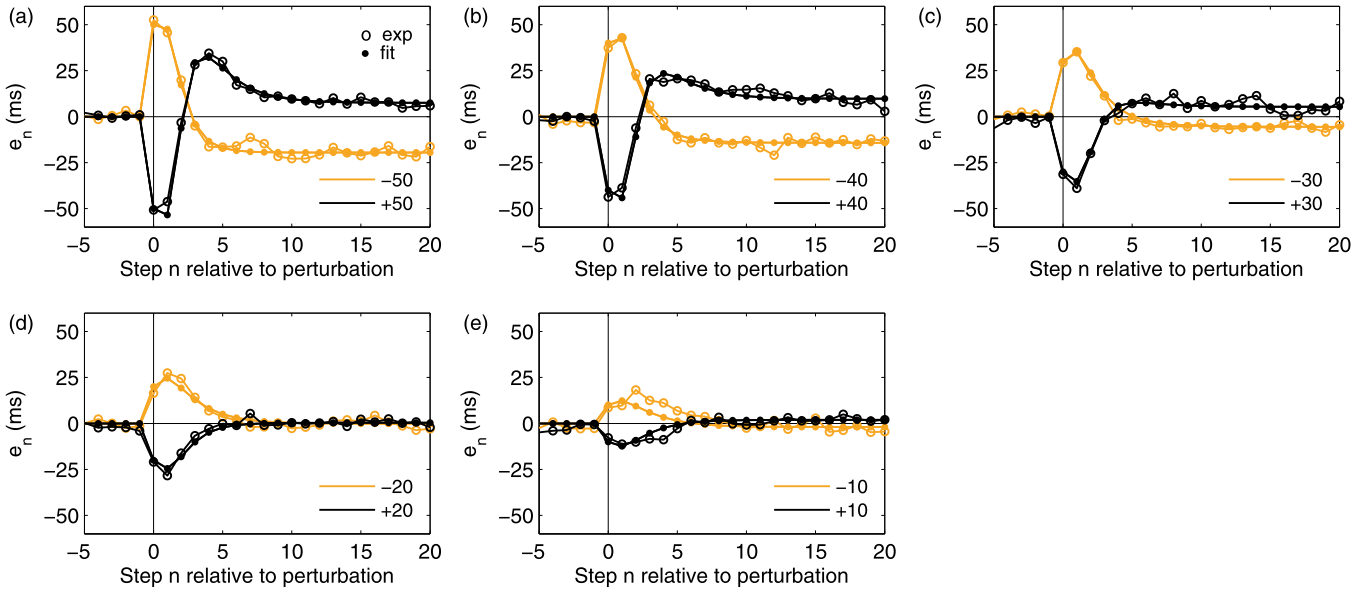

FIG. 9. Model fitting: Experimental time series vs. fitted time series. The obtained set of coefficient values is displayed in Table I.

APPENDIX: METHODS AND PARAMETER DISTRIBUTIONS

1. Estimation of return points

The return points of a map $e_{n+1} = f(e_n)$ are the values e_n such that $e_{n+1} = e_n$ (the analogous concept in a continuous-time flow is the nullcline, that is, the points in phase space where the rate of change associated to a given variable is zero). In the time series e_n the return points appear as local maxima or minima.

In a two-dimensional map:

$$\begin{aligned} e_{n+1} &= f(e_n, x_n) \\ x_{n+1} &= g(e_n, x_n), \end{aligned} \tag{A1}$$

the return points for the variable e_n are the solutions of the implicit function $e_n = f(e_n, x_n)$ and for the variable x_n are the solutions of the implicit function $x_n = g(e_n, x_n)$. Here it is clear that the return points give us information about the shape of f and g.

In our case we want to find the return points in the chosen bidimensional embedding $(e_n; z_n)$, where $z_n = e_n - e_{n-1}$. That is, on the one hand we want the points $(e_n; z_n)$ such that e_n is a local maximum or minimum (return points for the variable e_n) and on the other hand the points $(e_n; z_n)$ such that z_n is a local maximum or minimum (return points for the variable z_n).

We exemplify the procedure with the calculation for the variable e_n (see Fig. 8):

(i) Define a 5-point time window from $n = 0$ through $n = 4$;

(ii) Fit a fourth-order polynomial to the e_n time series in such window;

(iii) Find the local maximum or minimum e_{ret} of the fitted function and the corresponding value n_{ret};

(iv) Interpolate the z_n time series with a polynomial of the same order and compute the value $z(e_{\text{ret}})$;

(v) The return points are the set of values $(e_{\text{ret}}; z(e_{\text{ret}}))$.

Same procedure applies for the variable z_n after switching $e_n \leftrightarrow z_n$.

2. Genetic algorithm

We fitted the model to the data by using a genetic algorithm in C with both custom-written code and the GAUL libraries [37].

The eight model parameters were arranged into a single chromosome with eight genes and were initialized randomly from a uniform distribution in the ranges $-1.0 < a, b, c, d < 1.0$, $-0.01 < \delta < 0.01$, and $-0.0001 < \alpha, \beta, \gamma < 0.0001$. The number of generations was 200, the population size 2000, the crossover rate 0.9, and the mutation rate 0.1.

The fitness function was defined as minus the square root of the average squared deviation between model series and experimental series:

$$F = -\sqrt{\frac{1}{10 \times 26} \sum_{j=1}^{10} \sum_{n=-5}^{20} \left(e_n^j - E_n^j\right)^2 + P}, \tag{A2}$$

where e_n^j are the experimental time series and E_n^j are the model time series plotted in Fig. 9; $n = -5, \ldots, 20$ is the step number, and $j = 1, \ldots 10$ represents the 10 conditions -50, -40, -30, -20, -10, $+10$, $+20$, $+30$, $+40$, $+50$ ms used to fit the model. The fitness function F decreases as the differences $e_n^j - E_n^j$ get larger in absolute value. Note that fitting and simulations in this work encompass all steps $n = -5, \ldots, 20$, including the perturbation step $n = 0$ as shown in Fig. 3(a), making no distinction whatsoever among preperturbation, perturbation, and postperturbation.

In order to prevent survival of unrealistic solutions (for instance damped oscillations or alternating series), penalties were included as a positive term P inside the square root that depends on the linear coefficients only and takes a large value in any of the following cases:

(i) the eigenvalues are complex (in order to avoid oscillatory approach to the equilibrium);

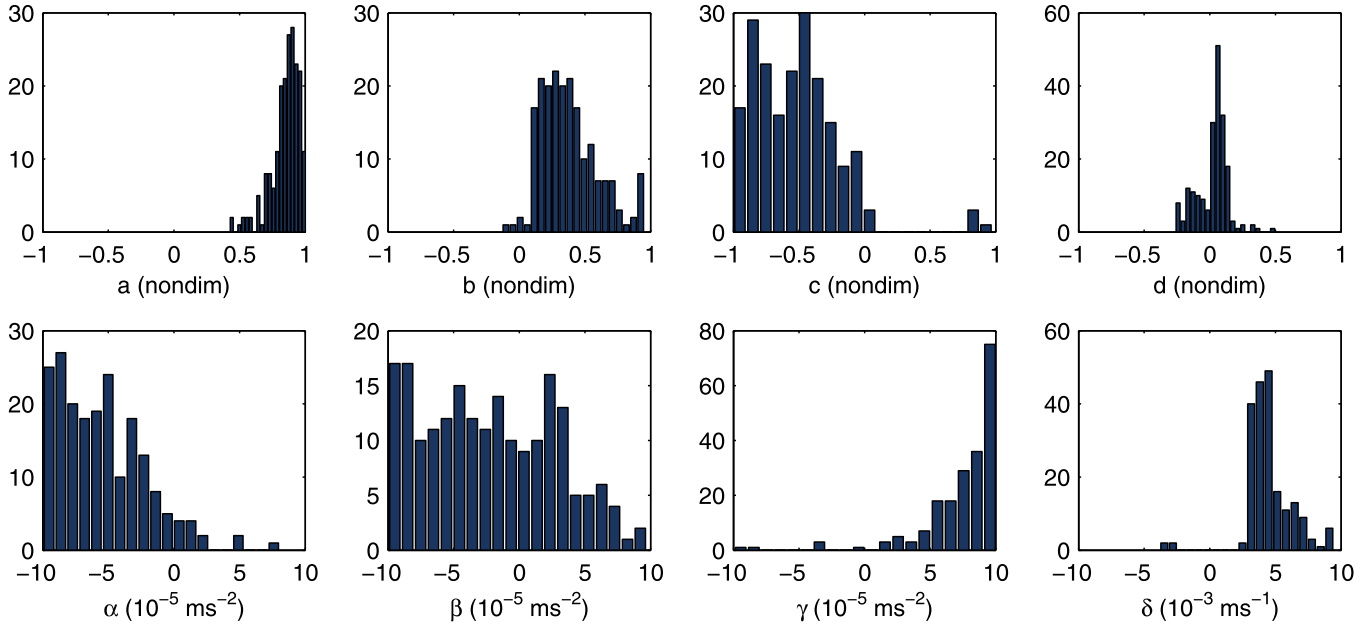

FIG. 10. Distribution of parameter fitted values.

(ii) the eigenvalues are real but any of them is either greater than 1 or negative (in order to avoid solutions with unstable manifolds, and convergent solutions that alternate sides);

otherwise, $P = 0$.

In order to prevent the selection of a surviving local optimum and to perform a statistical and dynamical study of the obtained solutions, the whole procedure described so far was repeated 200 times; the chosen solution was the one with the highest fitness of all.

To improve fitting, a postperturbation constant baseline was added to the model variable p_n with a fixed value equal to the experimental postperturbation baseline of the corresponding perturbation size.

3. Fitting results from all perturbation sizes

Figure 9 shows all experimental time series used for the fitting procedure (perturbation sizes ±50, ±40, ±30, ±20, and ±10 ms) and the corresponding model time series.

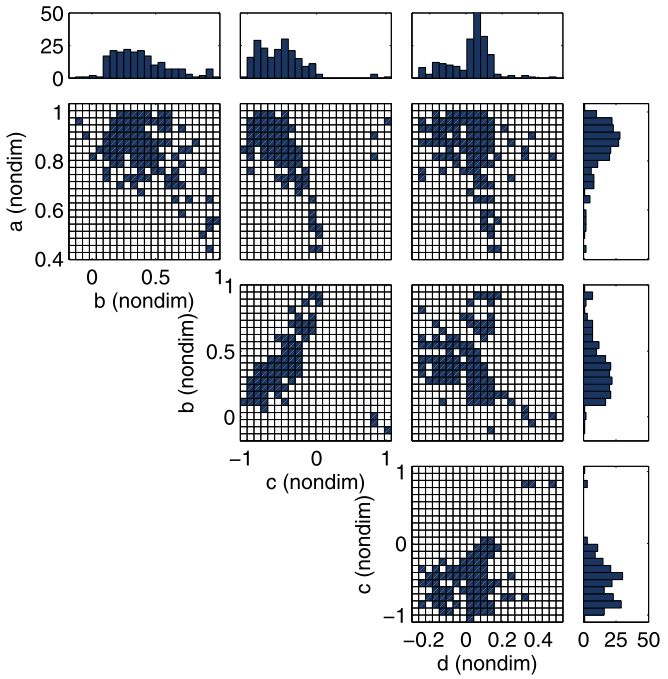

FIG. 11. Joint distributions of linear parameter values.

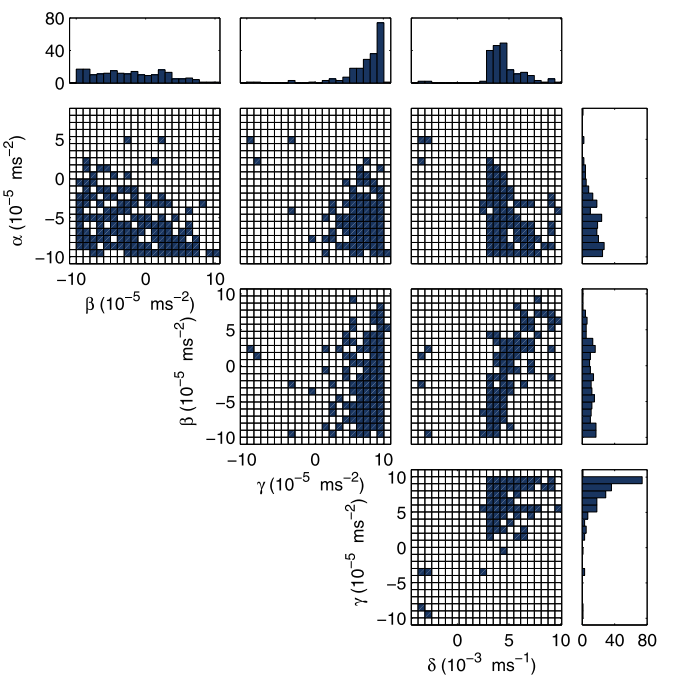

FIG. 12. Joint distributions of nonlinear parameter values.

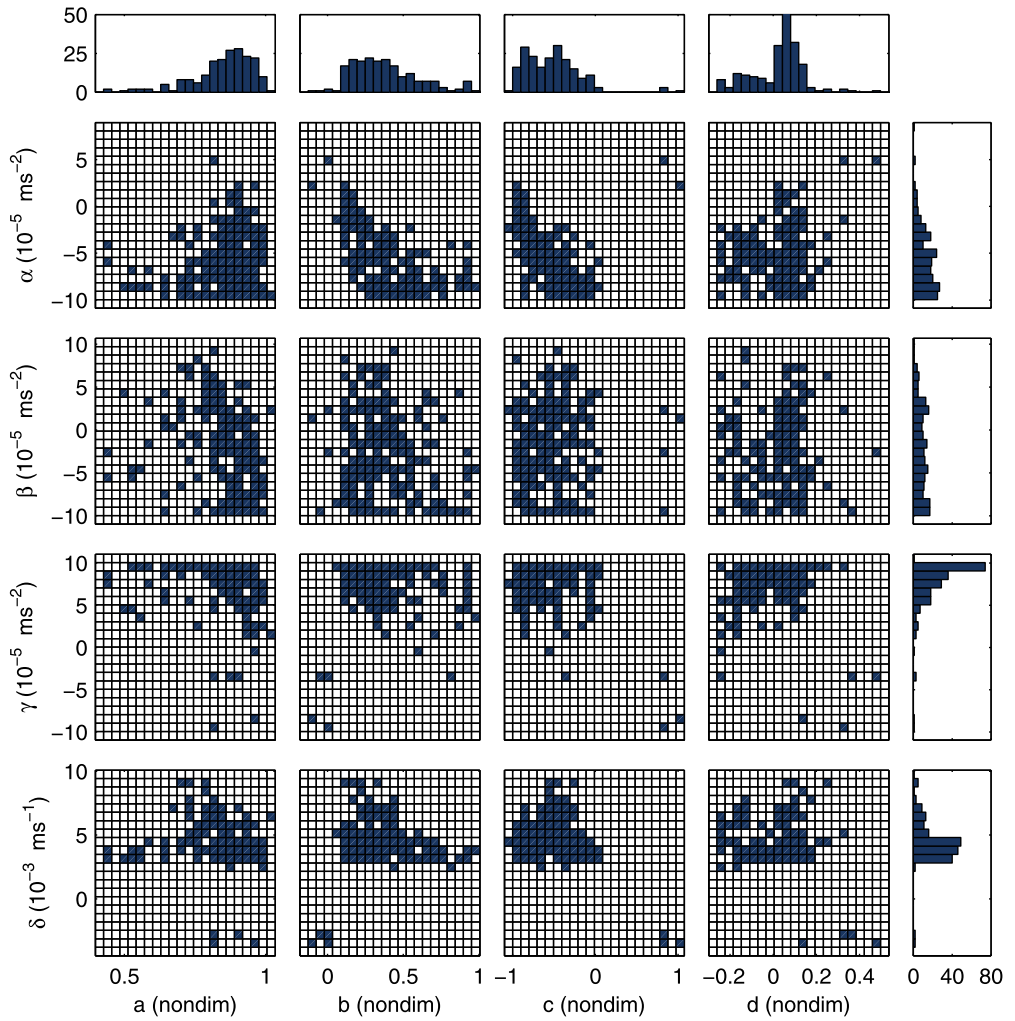

FIG. 13. Joint distributions of linear vs. nonlinear parameter values.

4. Fitted parameter distributions

See Figs. 10, 11, 12, and 13.

5. Parameter values of Type-II and Type-III phase spaces

See Tables II and III.

6. Data and code

See Supplemental Material [38] or at the Sensorimotor Dynamics Lab's webpage [39] for C and MATLAB code to reproduce all figures and data in this work.

We use the morgenstemning colormap [40] for color blind-friendly and grayscale-friendly plots.

TABLE II. Fitted parameter values for a representative solution of Type-II phase space [Fig. 4(b)]. Units as in Table I.

$a = 0.801$	$\alpha = -8.04 \times 10^{-5}$
$b = 0.699$	$\beta = -8.06 \times 10^{-5}$
$c = -0.220$	$\gamma = 9.76 \times 10^{-5}$
$d = 0.0167$	$\delta = 3.48 \times 10^{-3}$

TABLE III. Fitted parameter values for a representative solution of Type-III phase space [Fig. 4(c)]. Units as in Table I.

$a = 0.915$	$\alpha = 8.06 \times 10^{-5}$
$b = -0.0550$	$\beta = -9.22 \times 10^{-6}$
$c = 0.861$	$\gamma = -3.48 \times 10^{-5}$
$d = 0.364$	$\delta = -2.77 \times 10^{-3}$

[1] B. H. Repp, Psychon. Bull. Rev. **12**, 969 (2005).
[2] R. B. Ivry and R. M. Spencer, Curr. Opin. Neurobiol. **14**, 225 (2004).
[3] A. Schachner, T. F. Brady, I. M. Pepperberg, and M. D. Hauser, Curr. Biol. **19**, 831 (2009).
[4] A. D. Patel, J. R. Iversen, M. R. Bregman, and I. Schulz, Curr. Biol. **19**, 827 (2009).
[5] A. Hasegawa, K. Okanoya, T. Hasegawa, and Y. Seki, Sci. Rep. **1**, 120 (2011).
[6] B. H. Repp and Y. H. Su, Psychon. Bull. Rev. **20**, 403 (2013).
[7] Y. Chen, M. Ding, and J. A. Scott Kelso, Phys. Rev. Lett. **79**, 4501 (1997).
[8] B. H. Repp, J. Mot. Behav. **35**, 355 (2003).
[9] L. Bavassi, J. E. Kamienkowski, M. Sigman, and R. Laje, Psychol. Res. **81**, 143 (2017).
[10] P. Praamstra, M. Turgeon, C. W. Hesse, A. M. Wing, and L. Perryer, Neuroimage **20**, 1283 (2003).
[11] B. Pollok, J. Gross, D. Kamp, and A. Schnitzler, J. Cogn. Neurosci. **20**, 828 (2008).
[12] J. D. Bijsterbosch, K. H. Lee, M. D. Hunter, D. T. Tsoi, S. Lankappa, I. D. Wilkinson, A. T. Barker, and P. W. Woodruff, J. Cogn. Neurosci. **23**, 1100 (2011).
[13] S. Nozaradan, M. Schonwiesner, P. E. Keller, T. Lenc, and A. Lehmann, Eur. J. Neurosci. **47**, 321 (2018).
[14] K. J. Jantzen, B. R. Ratcliff, and M. G. Jantzen, J. Motor Behav. **50**, 235 (2018).
[15] J. R. Iversen and R. Balasubramaniam, Curr. Opin. Behav. Sci. **8**, 175 (2016).
[16] H. Merchant, J. Grahn, L. Trainor, M. Rohrmeier, and W. T. Fitch, Philos. Trans. R. Soc. Lond., B, Biol. Sci. **370**, 20140093 (2015).
[17] M. L. Bavassi, E. Tagliazucchi, and R. Laje, Hum. Move. Sci. **32**, 21 (2013).
[18] M. C. van der Steen and P. E. Keller, Front. Hum. Neurosci. **7**, 253 (2013).
[19] J. Pressing and G. Jolley-Rogers, Biol. Cybern. **76**, 339 (1997).
[20] E. J. Wagenmakers, S. Farrell, and R. Ratcliff, Psychon. Bull. Rev. **11**, 579 (2004).
[21] S. L. López and R. Laje, Sci. Rep. **9**, 17814 (2019).
[22] G. Schoner, Brain Cogn **48**, 31 (2002).
[23] R. Gilmore, Rev. Mod. Phys. **70**, 1455 (1998).
[24] M. H. Thaut, R. A. Miller, and L. M. Schauer, Biol. Cybern. **79**, 241 (1998).
[25] B. H. Repp, Hum Mov Sci **20**, 277 (2001).
[26] B. H. Repp and P. E. Keller, Q. J. Exp. Psychol A **57**, 499 (2004).
[27] H. H. Schulze, A. Cordes, and D. Vorberg, Mus. Percept. **22**, 461 (2005).
[28] E. W. Large, P. Fink, and J. A. Kelso, Psychol. Res. **66**, 3 (2002).
[29] B. H. Repp, P. E. Keller, and N. Jacoby, Acta Psychol. (Amst.) **139**, 281 (2012).
[30] H. Haken, J. A. Kelso, and H. Bunz, Biol. Cybern. **51**, 347 (1985).
[31] J. D. Loehr, E. W. Large, and C. Palmer, J. Exp. Psychol. Hum. Percept. Perform. **37**, 1292 (2011).
[32] S. W. Egger, N. M. Le, and M. Jazayeri, bioRxiv, 712141 (2019).
[33] G. Aschersleben and W. Prinz, J. Mot. Behav. **29**, 35 (1997).
[34] A. M. Wing, J. Exp. Psychol. Hum. Percept. Perform. **3**, 175 (1977).
[35] P. Q. Pfordresher and S. Dalla Bella, J. Exp. Psychol. Hum. Percept. Perform. **37**, 566 (2011).
[36] J. Mates and G. Aschersleben, Acta Psychol. (Amst.) **104**, 29 (2000).
[37] http://gaul.sourceforge.net.
[38] See Supplemental Material at http://link.aps.org/supplemental/10.1103/PhysRevE.100.062412 for all data, code, and instructions to reproduce all figures in the manuscript.
[39] www.ldsm.web.unq.edu.ar/perturbations2019.
[40] M. Geissbuehler and T. Lasser, Opt. Express **21**, 9862 (2013).